

BIO02: Backscattering Dark-Field Microscopy for Malaria Detection

Megan Kinniment

Supervisor: Professor Richard Berry

Abstract

A backscattering dark field microscope setup is optimized for the diagnosis of malaria via the detection of hemozoin, a crystal produced by malarial parasites. An optimum back focal plane (BFP) mask is recommended for maximising signal from hemozoin and minimising other sources of depolarised backscattering in thin smears and in an approximation of a thick smear. Discrete dipole approximation and Mueller calculus is used to obtain theoretical depolarised backscattering distributions for hemozoin and red blood cells, respectively. Thin and thick smears are shown to be better sample formats than flow channels for a hemozoin detecting diagnostic device. Off-axis illumination of the sample is explored as a potential way to improve signal-to-noise ratios by moving backscattering and specular reflection centers apart in the BFP. Sources of unexpected noise within the BFP of the off-axis setup are investigated and eliminated. The off-axis illumination setup is demonstrated by taking dark field images of infected thin smears.

1 Introduction

Malaria is a treatable, well studied disease that remains a significant cause of death globally. In 2018, it was estimated that there were 228 million cases of malaria worldwide and 405,000 associated deaths¹. Young children are particularly badly affected by malaria, with children under five making up 57% of deaths due to malaria in 2017². Unfortunately, diagnosing malaria clinically is often difficult due to early-stage infections presenting either no or very non-specific symptoms. The development of better diagnostic equipment plays an important role in the effort to reduce the burden of malaria. For example, by minimising the occurrence of drug resistant malaria (which is more common in areas where people take antimalarials when they do not have malaria), gathering information for large scale control strategies and diagnosing malaria in individuals so that they can be treated promptly.

Currently, there are two main methods of malaria diagnosis, light microscopy and rapid diagnostic tests (RDTs). Light microscopy involves the use of a microscope by a trained specialist to scan stained blood samples for markers of malaria infection, the detection threshold for light microscopy is 50-100 parasites per μl or higher in field settings³. Due to the lack of infrastructure in many places with high prevalence of malaria, light microscopy is often not used in favor of RDTs. RDTs work by detecting malarial antigens and are cheap, disposable tests that are ideal for use in areas without access to electricity or clinics with trained personnel. However, the sensitivity of RDTs is markedly below that of light microscopy, detecting $\leq 95\%$ of infected samples with parasitic loads of 1000-2000 parasites per μl)⁴.

The optical properties of hemozoin, a crystal produced by malarial parasites in red blood cells, could be used to create an improved RDT, with a sensitivity far exceeding that of current, antigen based RDTs. All *Plasmodium* species that cause malaria in humans infect red blood cells (RBCs). Within the RBCs, the

parasites consume hemoglobin, creating large quantities of heme as a waste product, which is highly toxic. The parasites convert this toxic free heme into the inert crystal hemozoin, in order to prevent damage to themselves and their host cell⁵. As a result, all RBCs infected with malaria contain hemozoin. Hemozoin is a crystal that scatters and depolarises light to a much greater extent than other substances in blood, particularly at angles far from the optical axis (especially the backward hemisphere). By looking only at backscattered, depolarised light it is possible to resolve scattering due to the presence of hemozoin in blood samples.

A cheap device for specifically detecting backscattered, depolarised light is shown in a 2016 paper by Robert Ishmukhametov et al. and is called a Back Scattering Dark Field Microscope (BSDF) with cross polarisers⁶. BSDF microscopes with cross polarizing filters are a very promising route for cheap and sensitive diagnosis of malaria because these microscopes only detect the depolarised, backscattered light that hemozoin very strongly produces relative to other components of blood. Currently, we are working with a company to begin the production of a prototype malaria diagnostic device for clinical use, which uses a miniature BSDF microscope to detect hemozoin. The purpose of this report is to inform the design and development of this prototype device by exploring ways in which the sensitivity to hemozoin of the BSDF setup can be improved.

Throughout this report, the depolarised backscatter detected from hemozoin will be referred to as “signal” and all light that reaches the camera from sources other than hemozoin will be referred to as “noise”. I am using depolarised to mean the light that is polarised perpendicular to the initial polarization of the light incident on the sample.

To improve the signal-to-noise ratio (SNR) of the BSDF setup two routes are explored. Firstly, by blocking light that has left the sample at certain angles from the optical axis using a mask, specifically angles of light that have very low SNRs due to con-

taining a large amount of noise, overall SNR can be improved. In order to find the optimum mask, depolarised angular backscattering distributions for hemozoin and various noise components are needed. Additionally, within this report depolarised backscattering angular distributions will be referred to as simply “scattering distributions” as light that is not both depolarised and backscattered (or reflected) is not detected by the BSDF setup. These scattering distributions are obtained via computational or experimental means. Optimum masking is mainly investigated within the original BSDF setup, referred to as the “on-axis illumination” setup or “on-axis” setup. For the on-axis setup a masking configuration optimising for both overall SNR and total signal detected is recommended for thin smear (monolayer of RBCs) and thick smear (lysed, or burst RBCs) sample formats.

Secondly, a slightly modified BSDF setup using off-axis illumination (the “off-axis” setup), is presented. The off-axis setup is able to separate specular reflections from backscatter. All specularly reflected light is noise since hemozoin does not specularly re-

flect any significant amount of light. Backscattered light can be both signal from hemozoin or noise from other backscattering components of a sample. In the on-axis setup, scattering angles with low SNRs due to specular reflections are completely removed via masking, along with any signal present. However, using an off-axis setup, the noise due to specular reflections can be removed without removing any signal, potentially allowing much greater overall SNRs to be achieved than with an on-axis setup.

Finally, the off-axis illumination setup is demonstrated by taking dark and bright field images of infected thin smears with a back focal plane (BFP) mask. Small regions of localised depolarised backscatter coinciding with positions of RBCs are observed within infected thin smears but not healthy thin smears, suggesting that the source of these regions of depolarised backscatter is hemozoin.

2 Method

2.1 On-Axis Experimental Setup

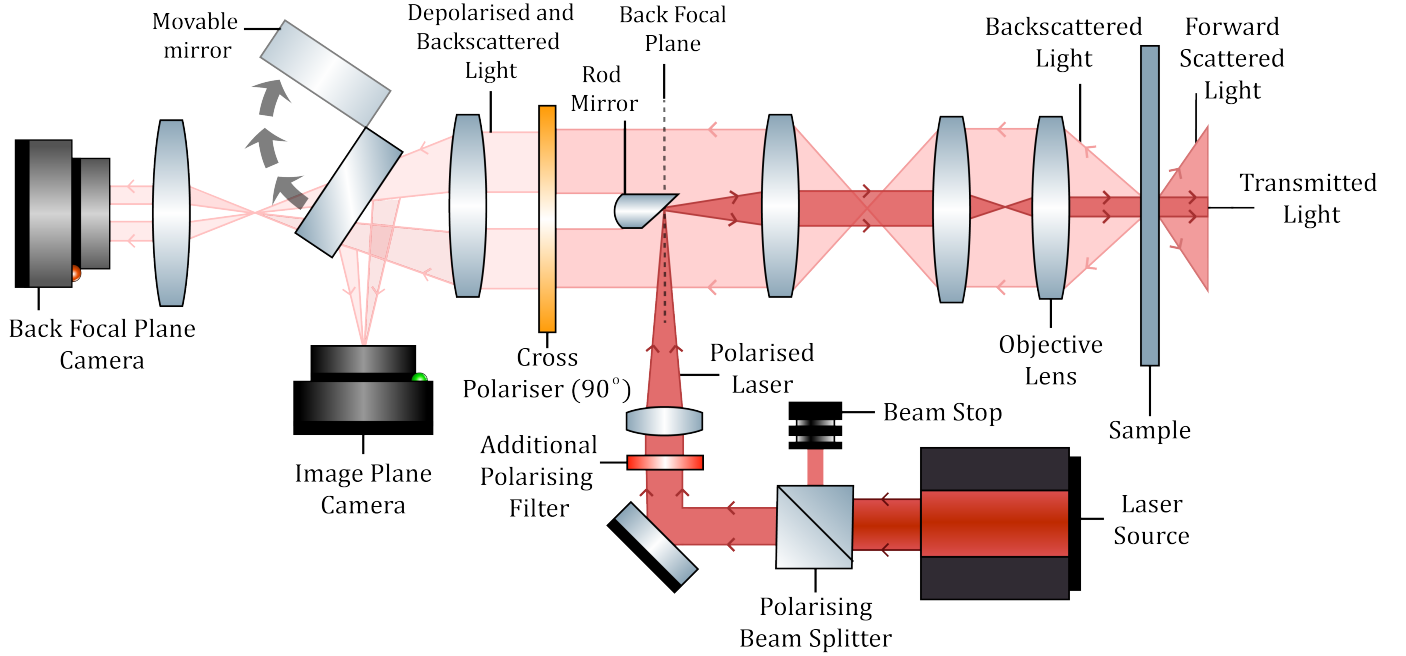


Figure 1: The Back Scattering Dark Field Setup with Cross Polarisers is shown in on-axis illumination mode. The laser is polarised, then redirected towards the sample by the rod mirror. Not pictured is light that is specularly reflected from the lenses. Light that is specularly reflected from the sample will, ideally, go back along the same path as the incident beam and be blocked by the rod mirror. Light that is specularly reflected from the lenses may travel any number of paths and is likely to be imaged by the BFP camera.

In the on-axis setup, the angular distribution of the depolarised backscatter from the sample was measured using a BSDF microscope with cross polarisers. Certain angles of light backscattered or reflected from the sample were removed by blocking areas of the beam within the plane of the rod mirror. An optimum size of the rod mirror exists for which overall SNR can be maximised.

To measure the depolarised backscatter of a sample a BSDF microscope with cross polarisers was used. The on-axis setup is pictured in Fig.1, lens focal distances are given in Fig.8 in the appendix. Polarised light with a wavelength of 632nm was shone onto a rod mirror which redirects the light through a series of lenses. The incident polarised light is collimated and parallel to the optical axis when it hits the

sample. Most of the incident light is either transmitted or forward scattered by the sample and leaves the setup. However, a small fraction of the incident light is backscattered or reflected by various components of the sample. The backwards travelling cone of light is collected up to angles from the optical axis equal to the angular aperture of the objective lens (θ_{lens}) and forms the backward traveling beam.

It should be noted that the objective lens is not actually a commercial objective but a simple aspheric lens. Simple aspheric lenses are used over commercial objectives because they are cheaper, more representative of the components likely to be used in the prototype diagnostic device and contain much fewer pieces of glass, greatly reducing depolarised light produced by interactions with the lenses. Two different simple aspheric lenses are used as the objective lens in this paper, with two different numerical apertures (NA). The numerical aperture of a lens is defined by $NA = n \sin(\theta_{lens})$, where n is the medium (in this case, air) and θ_{lens} is the angular aperture of the lens. A NA 0.53 lens with a 5mm focal length (giving 40x magnification) and a NA 0.26 lens with a 11mm focal length (giving 20x magnification) are used in this report.

The backwards travelling beam contains both backscattered and reflected light. The backscattered light contains both noise and some signal, since many other components of the sample produce backscatter, in addition to hemozoin. The reflected light is all noise because it is not a result of light interacting with hemozoin (with most reflected light arising from interactions with the coverslip and the slide). The backscattered and reflected light that makes up the beam continues through the setup, as shown in Fig.1, and will pass through the plane of the rod mirror. The rod mirror is placed such that it sits in the back focal plane of the nearest lens in the direction of the rod mirror (and will be referred to as simply the back focal plane or BFP throughout this report) and blocks the central area of the beam. Ideally, the rod mirror will completely block any specular reflections originating from the sample, allowing only backscattered light (and specular reflections from the lenses or other sources) to reach the cameras. This is because any specular reflections originating from the sample would ideally follow the same path as the incident beam and will be focused down to the center of the rod mirror in the BFP. However, it should be noted that in reality a substantial amount of specular reflections stray from this path and are not blocked by the rod mirror.

Within the BFP, the backward traveling beam is the Fourier Transform of the image of the sample. Physically this means that, within the BFP, the radial position of the light within the beam corresponds to the angle from which the light left the sample. The

light in the very center of the beam corresponds to light that left the sample parallel to the optical axis. The edges of the beam correspond to the maximum angle of light that is able to be collected by the objective lens.

In order to easily discuss the angular backscattering distributions of various samples and components, I will define a “backscattering angle”. This measures angles relative to the line parallel and in the opposite direction of the incident beam. For example, in the on-axis setup shown in Fig.1 light reflected back towards the rod mirror and normally to the sample, has a backscattering angle of 0 degrees.

The relationship between radial position in the beam as it travels through the BFP and the light's original backscattering angle forms the basis by which certain angles of light can be removed. As stated previously, the ability to remove certain angles of light from the beam has the potential to greatly increase overall SNR by allowing the removal of light at backscattering angles with very low SNRs. By varying the size of the rod mirror (the mask), light up to some radial position within the beam is blocked, corresponding to light up to some backscattering angle being blocked.

The beam then continues after masking by the rod mirror, now ideally containing only backscattering, through a polarising filter orientated perpendicular to the polarisation of the incident beam. As a result, only backscatter that is also depolarised can continue through the setup and be imaged by one of the cameras. Two cameras are used, one for capturing the image plane and one for the back focal plane. The movable mirror shown in Fig.1 can be flipped in or out to switch which plane is captured. The vast majority of data collection is performed with the BFP camera, as this is the plane that contains the depolarised angular scattering distribution information. The image plane camera is present mainly to aid with aligning and examining samples before data collection with the BFP camera.

Ideally, this setup allows only depolarised backscatter to reach the cameras and the rod mirror completely blocks all specular reflections. The rod mirror acts as a mask within the BFP, blocking light. By blocking backscatter up to some radial position in the beam, light with corresponding backscattering angles can be removed up to some angle.

2.2 Finding an Optimum Back Focal Plane Mask for the On-Axis Setup

An example of a BFP image can be seen in Fig.2, the sample is isotonic buffer which is not expected to produce any significant backscattering but is expected to show components of depolarised light from reflections from the slide, coverslip and lenses within the

setup. A comparison of the BFP image of a monolayer of infected RBCs, which does produce significant backscattering, and of isotonic buffer is shown in Fig.9 in the appendix. The rod mirror acts both to redirect the polarised laser towards the sample and to block light within the central portion of the backward traveling beam. Within the BFP, the light's radial position in the beam corresponds to the angle at which the light left the sample. By increasing the size of the rod mirror, a larger central area of the beam is blocked. The light with the smallest radial position that is not blocked by the mirror corresponds to the minimum backscattering angle for which light can reach the cameras (θ_{mask}). Light with the largest radial position (which is limited by the angular aperture of the objective lens, θ_{lens}) corresponds to the maximum backscattering angle for which the light can reach the cameras.

Example On Axis BFP Image of an Infected Thin Smear with NA 0.53 Lens

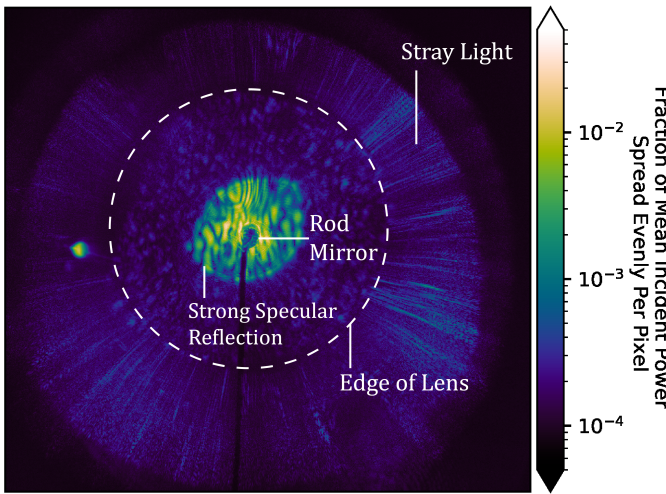


Figure 2: A BFP image of an isotonic buffer sample taken in on-axis mode with the NA 0.53 lens. The power at every pixel in the image is measured as a fraction of the power incident on the sample if that power were spread evenly across every pixel in the image. A large region of strong specularly reflected light can be seen with the very central part being blocked by the rod mirror. Stray light is light that reaches the camera without going through the objective lens.

In order to maximise overall SNR and sensitivity to hemozoin signal, the size of the rod mirror (the central mask) is chosen according to two criteria. Firstly, maximisation of average SNR across all unblocked angles. Secondly, to maximise total signal present across all unblocked angles. This second criterion devalues masks that only let a very narrow range of backscattering angles through, this increases the robustness of the recommended optimum mask if there are small errors in the predicted SNR profiles and potentially increases sensitivity to hemozoin. These two criteria are combined to a produce a score for finding the optimum central mask size for any signal-to-noise

ratio as a function of backscattering angle:

$$S(\theta_{mask}) = \underbrace{\frac{\int_{\theta_{mask}}^{\theta_{lens}} SNR(\theta)d\theta}{\theta_{lens} - \theta_{mask}}}_{\text{Mean Unmasked SNR}} \cdot \underbrace{\frac{\int_{\theta_{mask}}^{\theta_{lens}} SNR(\theta)d\theta}{\int_0^{\theta_{lens}} SNR(\theta)d\theta}}_{\text{Unmasked Fraction of Total SNR}}$$

This scores each mask size, where size is measured in terms of the maximum backscattering angles that such a mask would block. The size of mask that scores most highly is the optimum mask size. Due to the difficulty of determining exact concentrations of every scattering component within a sample it is very difficult to ascertain the exact relative magnitudes of the signal and all the different components of noise. This score is unaffected by the exact magnitude of the signal and noise components, only comparing the scattering distribution shapes, and so avoids this issue. In order to evaluate this score for every mask size, the depolarised angular backscattering distributions of both the signal and the noise must be known. No experimental data on the scattering distribution of hemozoin could be found so Discrete Dipole Approximation (DDA) simulations are used to obtain this. It is also not trivial to obtain the scattering distribution of the noise. Within a BFP image of a sample there exists many different components that contribute to noise. For example, an infected thin smear sample (a sample type that roughly produces a monolayer of RBCs) can be expected to have scattering components of: hemozoin, deformed RBCs, crenated RBCs (dried RBCs that have a spiked surface), monolayers of healthy RBCs, the slide, the coverslip and the lenses within the BSDF setup.

2.3 Obtaining Angular Scattering Distributions from Back Focal Plane Images

To find the angular scattering distribution of a sample from its BFP, the image is first radially averaged about the rod mirror, whose position in the BFP corresponds to a backscattering angle of 0 degrees. In the on-axis setup the position of the rod mirror also corresponds to the center of the BFP but this is not the case in the off-axis setup, which can be seen in Fig.3. The intensity is radially averaged to an intensity per pixel, so that increasing radii containing more pixels within the BFP are accounted for.

In order to obtain angular scattering distributions from the back focal plane images, a conversion between the radial position from the rod mirror (in pixels) and the backscattering angle the light left the sample at, needs to be found. The position of the rod mirror determines from what position the incident beam originates from the BFP. If the rod mirror is offset from the optical axis, the incident beam will originate from a different point in the BFP and hit the sample at an angle to the optical axis, this can

also be seen in Fig.3 within the diagram of the off-axis setup. A portion of the incident beam is transmitted straight through the sample and then hits a ruler placed a known distance from the sample, the distance the beam has travelled perpendicular to the optical axis can then be measured. The angle from the optical axis that the incident beam hit the sample is calculated using the two above distances and can be associated with the radial position of the rod mirror from the optical axis (in pixels) within the BFP. Light that is backscattered back along this path would then end up in the same position of the BFP as the current position of the offset rod mirror and have a backscattering angle equal to the calculated angle that the transmitted beam makes with the optical axis. This association between backscattering angle was then repeated for multiple radial positions within the BFP and this data was fit to a sine curve to obtain a conversion formula. This angle calibration was performed for each objective lens used.

An intensity calibration was performed to map pixel value to light intensity for the BFP camera. An Andor Neo sCMOS camera was used as the BFP camera. A laser was passed through a pinhole, shone directly onto the CMOS of the camera, and the power of the laser just before hitting the CMOS was measured. The total extra value of the pixels within the camera image when the laser was present was used to asso-

ciate pixel values to an absolute power being shone on the CMOS, linearity of the CMOS was assumed so that this can simply be extrapolated to other pixel values and intensities. Unless otherwise stated, the pixel value will be normalised such that if the power incident on the sample was spread evenly over the entire back focal plane image, each pixel value would be one.

2.4 Simulations

The depolarised angular scattering distribution of hemozoin was found using the DDA method, recreating the results of Wilson et al's 2011 paper⁷. Using the software DDSCAT, the parameters from the paper mentioned and a volume of $0.1\mu\text{m}^3$ for a single hemozoin crystal⁸, scattering distributions for a rectangular prism of aspect ratio 1:1:4 were obtained. Images of the full predicted depolarised scattering distribution for hemozoin is shown in the appendix in Fig.10. Only two cross sections of the full depolarized scattering distribution of hemozoin were obtained due to computational limitations. Depolarised scattering distributions for RBCs, both with light normally incident and randomly orientated, were obtained using Mueller calculus and Mueller matrix elements from the literature⁹.

2.5 Off-Axis Experimental Setup

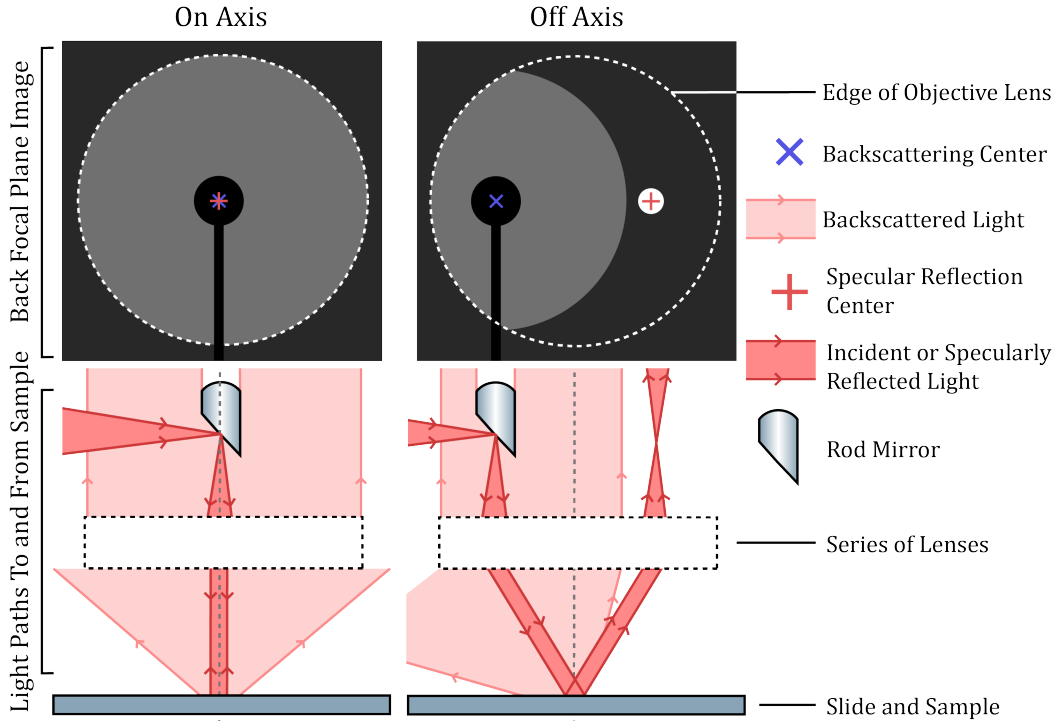


Figure 3: On-Axis and off-axis illumination modes are shown. In each diagram only backscattering up to some upper angle is shown for clarity. In reality backscattering will both extend past this angle and be angle dependent. The width of the “series of lenses” rectangle corresponds to the extent of the objective lens, light that falls outside of the extent of the objective will not be imaged by the setup.

A comparison of on-axis and off-axis illumination modes is shown in Fig.3. In the on-axis illumination mode the specular reflection and backscattering are centered around the optical axis of the setup (the middle of the BFP). Radial averaging of the on-axis BFP images about the center of backscattering (the center of the rod mirror) allows depolarised angular backscattering distributions to be found. Ideally, a mask size can be chosen to completely obscure any light appearing due to the lenses within the setup or reflections from the slide because these sources of noise tend to be centered sharply around a backscattering angle of 0 degrees. The more isotropic backscattering from hemozoin will then dominate the unmasked areas of the BFP, giving a high signal-to-noise ratio. The off-axis mode of illumination has advantages over the on-axis setup under two conditions. Firstly, if specular reflections have a large extent, particularly if the extent of these direct reflections overlaps with regions of strongest backscatter for hemozoin, then the hemozoin signal-to-noise ratio could be very small. Secondly, if the hemozoin signal-to-noise ratio is higher at angles of backscattering higher than the angular aperture of the objective lens. The first condition is relatively obvious, if noise from specular reflections is present in a large area of the BFP then a larger mask is required to remove the noise, therefore there is less unmasked area with which to detect hemozoin signal, lowering sensitivity. As a result, when very large areas of the BFP need to be masked due to specular reflections, it becomes advantageous to move the specular reflections to another part of the BFP, allowing separate masking and conserving backscattering signals. The second condition is a result of off-axis illumination allowing the imaging of light scattered at higher backscattering angles than the angular aperture of the lens. In Fig.3 a cone of backscattered light is shown for illustrative purposes but in reality backscattered light could be scattered at backscattering angles all the way up to 90 degrees. In both setups, light that does not enter the objective lens will not be collected. For the on-axis setup this means that any light that is backscattered further than the angular aperture of the objective lens will not be imaged. In the off-axis setup the backscattering center is moved such that light that previously would have been backscattered at too high of an angle to enter the objective now can be imaged. In the extreme, with the incoming laser placed at the very edge of the objective lens, this would result in being able to image backscattering angles up to twice that of the on-axis setup.

For two different objective lenses BFP images were collected for various samples. Healthy and infected thin smears were measured. Samples of rutile (a known depolarising isotropic scatterer) and flow channels of blood (for random orientations of RBCs)

were also used. BFP images were taken for both lenses in off-axis and on-axis modes. Backscattering and reflections from within the setup itself were also measured by taking pictures of the back focal plane without a sample.

3 Results and Discussion

3.1 On-Axis Results

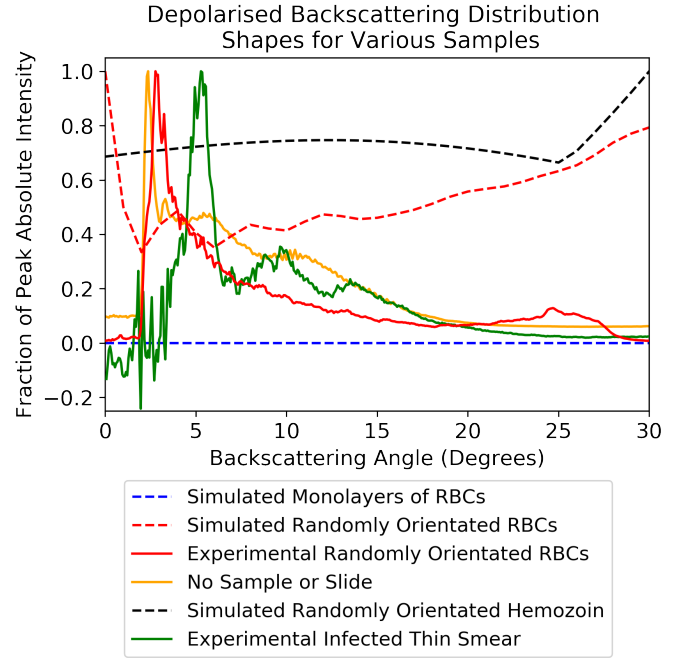


Figure 4: The depolarised backscattering distributions of various samples are shown for backscattering angles up to close to the angular aperture of the NA 0.53 lens (32 degrees). Experimentally obtained distributions are shown with solid lines and computationally obtained ones with dashed lines. All experimentally obtained distributions (apart from “No Sample or Slide”) have been subtracted by the distribution of a buffer only sample, to attempt to remove components of scattering due to the slide, coverslip and lenses within the BSDF setup. Each curve is normalised such that the absolute value of its peak within the angular range shown is one.

Angular depolarised scattering distributions were obtained for various samples and can be seen in Fig.4. Since the exact concentration of the relevant scattering components within each sample is difficult to ascertain, the relative magnitudes of different components of scattering can not be compared. Instead, each distribution is normalised to (the absolute value of) its own peak within this angular range to allow for comparison of the distribution shapes. The scattering distributions for the infected thin smear and randomly orientated RBCs have been subject to background subtraction. This means that these scattering distributions have been subtracted by the scattering distribution of an empty buffer sample to try and remove components of scattering due to the slide, the

coverslip and lenses within the setup.

The shapes of the experimental scattering distributions are significantly different from what is predicted by simulations of the components within these samples, suggesting that the shape of the experimental scattering distributions is dominated by different scattering components of the sample or interactions between these components. An experimental healthy thin smear sample was imaged but produced anomalous results and is not shown. Simulations of light incident normally on RBCs indicate that they do not produce depolarised backscattering at any angle, implying that very little noise will be produced by the monolayer of RBCs within a healthy thin smear in the on-axis illumination mode. In contrast, the healthy randomly orientated RBCs do produce a signal above that of a buffer sample, indicating that randomly orientated RBCs do contribute to backscattering. This has implications for which sample formats are best to use in a prototype BSDF malaria diagnostic device. Since randomly orientated healthy RBCs produce more backscattering than monolayers of healthy RBCs, flow channel sample formats that flow blood past the objective (randomising RBC orientation) will produce more noise and have lower SNRs than thin smear sample formats.

As detailed in the methods section, in order to decide on the optimum mask size a score was created based on maximising overall SNR and total signal detected. Ideally, the experimental scattering distribution of real samples of hemozoin would be used as the signal distribution. Since the experimental hemozoin scattering distribution is not known and it is also not possible to isolate the hemozoin scattering component of infected thin smears, an approximation of the hemozoin scattering distribution is used as the signal when finding the optimum mask size. The hemozoin scattering distribution is assumed to be completely isotropic over the angular range of the lens. This is motivated by two main observations.

Firstly, the simulated hemozoin scattering is close to isotropic over this angular range, only increasing significantly at backscattering angles above 26 degrees, see Fig.10 for full distribution in appendix. Secondly, it is likely that real hemozoin crystals will have more isotropic backscattering distributions than the simulations of hemozoin suggest. In the DDA simulations, hemozoin is modeled as a smooth rectangular prism whereas real hemozoin crystals have rough surfaces and stick together randomly, reducing the similarity of each hemozoin mass.

The noise distribution used to analyse SNR over backscattering angle ought to be representative of the noise that will be detected when the device scans real infected samples for hemozoin signal. Currently, there are two promising sample formats for this device, thin smears and thick smears. Infected thin smear scattering distributions have already been obtained experimentally, see Fig.4. Thick smears are a sample type in which all RBCs (both healthy and infected) are burst, destroying the RBCs and freeing the hemozoin trapped inside. Thick smears are particularly promising sample formats for two main reasons. A much higher number of RBC contents can be examined per field of view compared to the RBC monolayers of a thin smear and secondly because the structure of the RBCs are destroyed, the RBC's themselves they are likely to produce little to no backscattering. Due to time constraints and limited supplies of infected blood, thick smear samples were not used. Within a thick smear sample the components of scattering due to healthy RBCs, crenated RBCs and infected RBCs will likely be small. As a result, infected thick smear sample scattering distributions are likely to be roughly equivalent to that of buffer samples, with an additional hemozoin scattering component (the signal). So, to attempt to predict the optimum mask size for thick smears, the scattering distribution of a buffer sample is used as the noise component.

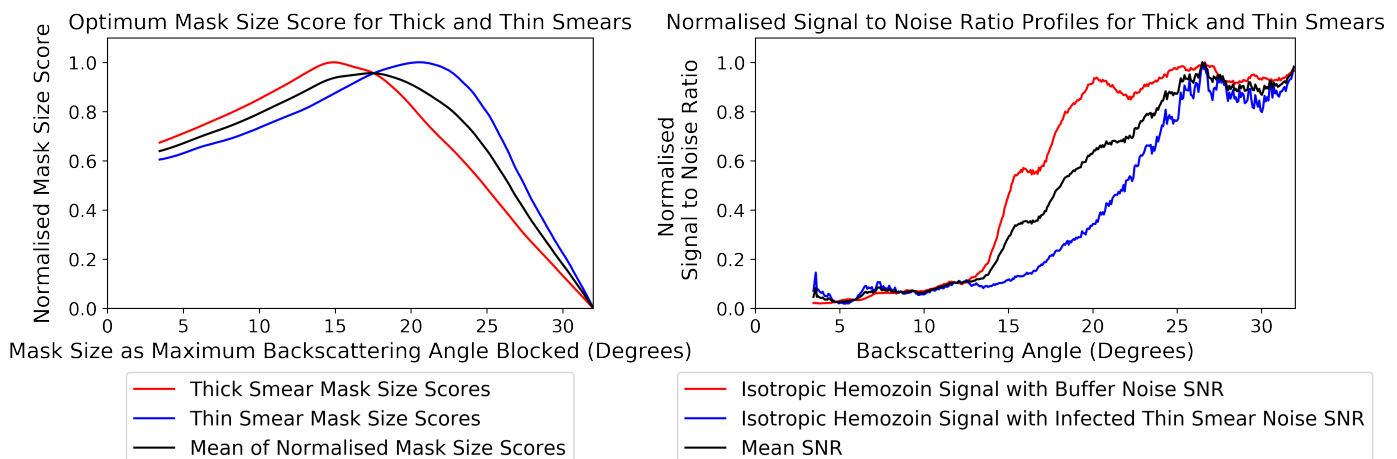


Figure 5: SNRs and Optimum Mask Size Scores are shown for two signal and noise pairs. Both lines have an isotropic signal, approximating that of hemozoin. Both mask score lines and SNRs are normalised such that they peak at one. The line depicting mean of the two normalised mask size scores is not normalised again.

In Fig.5 the SNRs and mask size score curves are shown for two sample formats. The approximate isotropic hemozoin scattering distribution is used as the signal in both cases. The SNR profiles are not shown below a backscattering angle of three degrees due to the presence of the rod mirror at those angles. The experimental infected thin smear scattering distribution is used to represent noise from an infected thin smear. To approximate the angular noise distribution of an infected thick smear, a buffer sample is used. Note that the infected thin smear contains scattering components of experimental hemozoin. Since it is not possible to determine what scattering is produced by hemozoin and what is produced by other components, the infected thin smear scattering distribution being used as noise does actually contain some signal. However, as long as the experimental hemozoin scattering distribution and the isotropic scattering distribution used as the signal are sufficiently similar, the SNR will still be a good indicator of the backscattering angles at which the noise is least prevalent.

The SNRs and mask size scores are shown for an isotropic signal (hemozoin) and two different noise distributions, an experimental infected thin smear and a buffer sample (which is a likely approximation of an infected thick smear sample, excluding the scattering component caused by hemozoin). These mask size score curves show the score that a mask that blocked light all the way up to a particular backscattering angle would get for a given SNR profile. For example, the peak of the thin smear score curve lies at 20.4 degrees (9.5mm radius in our setup), indicating that the highest-scoring mirror (or mask) size for the thin smear is one that blocks all light that left the sample with a backscattering angle of less than 20.4 degrees. Similarly, the optimal mask size for the thick smear approximation as buffer is 14.9 degrees (7.0mm radius in our setup). The mean of these two SNRs is also shown in Fig.5 and the corresponding optimal mask size is 17.4 degrees (8.0mm radius in our setup).

3.2 Off-Axis Results

In the off-axis configuration, the intensity of backscattered signal varied significantly with the offset of the laser, even with no sample present, this can be seen in Fig.6. This suggests that when the lenses within the setup are illuminated at certain offsets, they are significant sources of depolarised light. All light detected by the BFP camera when no sample present is noise, mostly produced by the lenses within the setup.

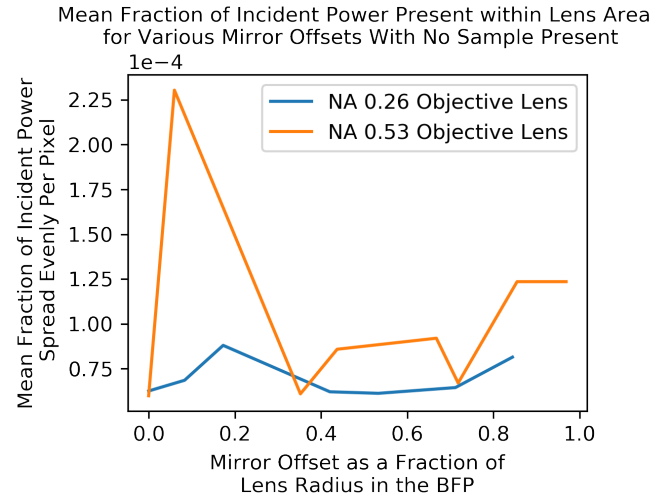


Figure 6: Mean power received by the BFP camera in a rectangular selection encompassing the lens and the rod mirror with no sample present.

The choice of objective lens had a significant effect on this lens noise observed, with the simple NA 0.53 lens giving particularly high levels of lens noise at certain rod mirror offsets. However, the quietest rod mirror offsets for both lenses produce a similarly low level of lens noise. For the off-axis setup, the NA 0.26 lens was used as the objective lens to increase the field of view of the setup and so that lens noise was less of an issue when picking a rod mirror offset. Off-axis experiments with samples were done with rod mirror offsets that both minimised the backscattering signal due to the lenses within the setup and maximised the laser offset so that the backscattering and direct reflection centers were separated as much as possible.

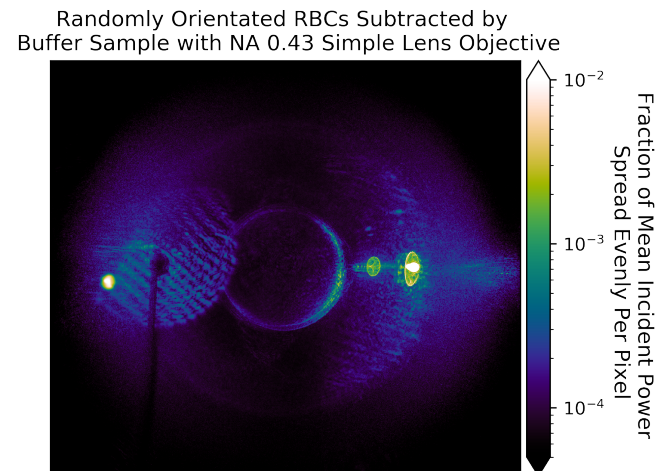


Figure 7: A BFP image of an RBC flow channel sample. The mirror can be seen on the left surrounded by backscatter close to the edge of the objective lens. Surrounding the edge of the lens is a penumbra of stray light. In the center the bright ring artifact can be seen. On the right are two bright specular reflections.

A back focal plane image for a healthy RBC flow

channel sample (randomly orientated RBCs) subtracted by an empty buffer sample with a NA 0.53 simple objective lens is shown in Fig.7. Depolarised backscatter was expected to be symmetric about the backscattering center, with a large amount of light in the vicinity of the area of specular reflections, which can be seen in Fig.7. The presence of an additional bright ring symmetric about the optical axis was not expected. The symmetry around the optical axis in the BFP images indicates that its source has symmetry about the direction normal to slide. Since the bright ring was initially seen in a sample containing a monolayer of RBCs (and these RBCs are symmetric about the normal to the slide) I initially expected that the bright ring was either produced by RBCs stuck flat to the slide or a lens edge effect. However, the bright ring was also observed when the edge of the objective lens was masked and in samples of rutile (a known isotropic depolarising scatterer), indicating that that the artifact was not a lens edge effect nor produced by monolayers of RBCs or even the RBCs themselves but instead by interactions between some angles of the backscattered light and the lenses within the setup. This was supported by the disappearance of the bright ring when changing the objective lens from the simple NA 0.53 to the simple NA 0.26 lens.

The existence of artifacts like the bright ring suggests that the lenses within the setup can modify the backscattering signal, in addition to simply adding to it in a manner that is easy to remove through subtraction by a buffer sample. A possible mechanism for this could be that some backscattered light enters internal reflection modes within the objective lens. Some of these modes may take light that enters them and partially polarise the light perpendicularly to the polarisation of the incident laser light, allowing more of this light to travel through the second polarising filter and increasing its intensity within the BFP. Additional depolarised backscatter due to internal reflection modes of the lens would be expected to be symmetric about the optical axis and is a possible explanation for the bright ring artifact. The observation that, when no sample is present, the NA 0.26 lens produces much less lens noise overall compared to when the NA 0.53 lens is used as the objective can also be explained via the reduction of internal reflections within less curved surfaces.

Finally, the off-axis illumination setup was used with a new BFP mask and a NA 0.26 objective lens to take dark field and bright field images of infected and healthy thin smears. Within infected thin smears localised regions of intense depolarised backscatter from within some infected RBCs (likely produced by hemozoin) were observed, these were not observed in healthy thin smears, two of these images are displayed in the appendix in Fig.11. Although, little can be concluded about the SNR of such a setup currently

(due to a lack of a sample with a known quantity of hemozoin and time constraints) these observations are very promising and are a preliminary indication that low power, cheap, simple objective lenses can replace commercial objectives in a diagnostic device.

4 Conclusion

For the on-axis illumination configuration, an optimum rod mirror size was predicted for the NA 0.53 lens for thin and thick smears using a hemozoin depolarised backscattering signal approximated to be isotropic up to the angular aperture of the objective lens. The optimal rod mirror size for thin smears blocked backscattering angles up to 20.4 degrees (9.5mm radius in our setup) and for thick smears up to 14.9 degrees (7.0 mm radius in our setup).

DDA simulations of the depolarised scattering distribution of a hemozoin-like rectangular prism predict that depolarised backscattering intensity is approximately constant over backscattering angles smaller than 26 degrees, then increases steadily and peaks at angles around 90 degrees, suggesting that off-axis setups that are able to access these higher backscattering angles will likely have increased SNRs. However, current theoretical depolarised scattering distributions for hemozoin have not been experimentally verified and may not be applicable to real hemozoin crystals due to clumping and uneven surfaces present within real hemozoin samples.

It was found that randomly orientated RBCs have a significant contribution to depolarised backscattering but monolayers of RBCs do not, suggesting that thin smear sample formats will provide superior SNRs compared to flow channel sample formats. Thick smears are an additional promising sample format because of the high numbers of RBC contents that can be analysed per field of view and the potential reduction in noise due to lysing of the RBCs.

Within the off-axis setup, it was found that even with no sample present, there was great variability in the intensity of noise produced when offsetting the rod mirror by different angles. With no sample, the NA 0.26 simple objective lens was observed to have fewer mirror offsets that produced a large amount of noise compared to the NA 0.53 lens, suggesting that lower power lenses produce less noise than higher power lenses.

When using the NA 0.53 objective lens in the off-axis illumination setup a bright ring artifact was observed around the center of the BFP and was deduced to be produced by light entering internal reflection modes within the objective lens. On changing the objective lens from the NA 0.53 lens to the NA 0.26 lens objective the bright ring disappeared.

Internal reflection modes within the lenses in the

off-axis setup, particularly the objective lens, offers a mechanism for both the extreme variability in lens noise observed with no sample present at different rod mirror offsets and for the source of the bright ring artifact observed with the NA 0.53 lens. The bright ring may not be present with the NA 0.26 objective lens because lower power lenses have less curved surfaces with fewer and weaker internal reflection modes. The variability in lens noise with no sample at different offsets may be due to the laser entering internal reflection modes within the lenses in the setup at certain offsets.

Dark field images with localised regions of intense depolarised backscatter (likely hemozoin) within some RBCs in infected thin smears provide a demonstration of the off-axis illumination setup with cheap, low power lenses (NA 0.26 simple aspheric) instead of commercial objectives.

Given more time on this project I would have liked to obtain experimental data on the noise produced by thick smears. I suspect lysed cells will produce a negligible amount of depolarised scattering and the increased volume of blood in each sample is likely to allow higher signal-to-noise-ratios for detection of hemozoin signal. I also would have liked to test any improvements to the on-axis illumination mode when the mask size I recommended is implemented and the exposure increased.

Finally, knowledge of experimental hemozoin scattering distributions would be incredibly valuable and would greatly help research within this area in general. Acquiring a positive control (pure hemozoin sample) would also be greatly useful, and would have allowed me to improve the certainty of my on-axis conclusions, as I would have a sample with which I could purely isolate the hemozoin scattering component. A positive control would also be extremely useful for finding the optimal mask for the BFP of an off-axis setup, where internal lens reflections, specular reflections and the lack of radial symmetry make predicting the optimum mask more difficult.

WORLD MALARIA REPORT, 2019.

- [2] Max Roser and Hannah Ritchie. Malaria - our world in data. *Our World in Data*, nov 2013.
- [3] Chansuda Wongsrichanalai, Mazie J. Barcus, Sinuon Muth, Awalludin Sutamihardja, and Walther H. Wernsdorfer. A review of malaria diagnostic tools: Microscopy and rapid diagnostic test (RDT) - defining and defeating the intolerable burden of malaria III: Progress and perspectives - NCBI bookshelf. *American Journal of Tropical Medicine and Hygiene*, 2007.
- [4] Anders Björkman and Andreas Maartensson. Risks and benefits of targeted malaria treatment based on rapid diagnostic test results. *Clinical Infectious Diseases*, 51(5):512–514, sep 2010.
- [5] Kim Y Fong and David W Wright. Hemozoin and antimalarial drug discovery. *Future medicinal chemistry*, 5(12):1437–1450, aug 2013.
- [6] Robert R Ishmukhametov, Aidan N Russell, Richard J Wheeler, Ashley L Nord, and Richard M Berry. A simple low-cost device enables four epi-illumination techniques on standard light microscopes. *Scientific Reports*, 6:20729, Feb 2016.
- [7] Benjamin K Wilson, Matthew R Behrend, Matthew P Horning, and Michael C Hegg. Detection of malarial byproduct hemozoin utilizing its unique scattering properties. *Optics Express*, 19(13):12190–12196, jun 2011.
- [8] Yulia M Serebrennikova, Janus Patel, and Luis H Garcia-Rubio. Interpretation of the ultraviolet-visible spectra of malaria parasite plasmodium falciparum. *Applied Optics*, 49(2):180–188, jan 2010.
- [9] Lei Bi and Ping Yang. Modeling of light scattering by biconcave and deformed red blood cells with the invariant imbedding t-matrix method. *Journal of Biomedical Optics*, 18(5):55001, may 2013.

References

- [1] WHO Global Global Malaria Programme.

5 Appendix

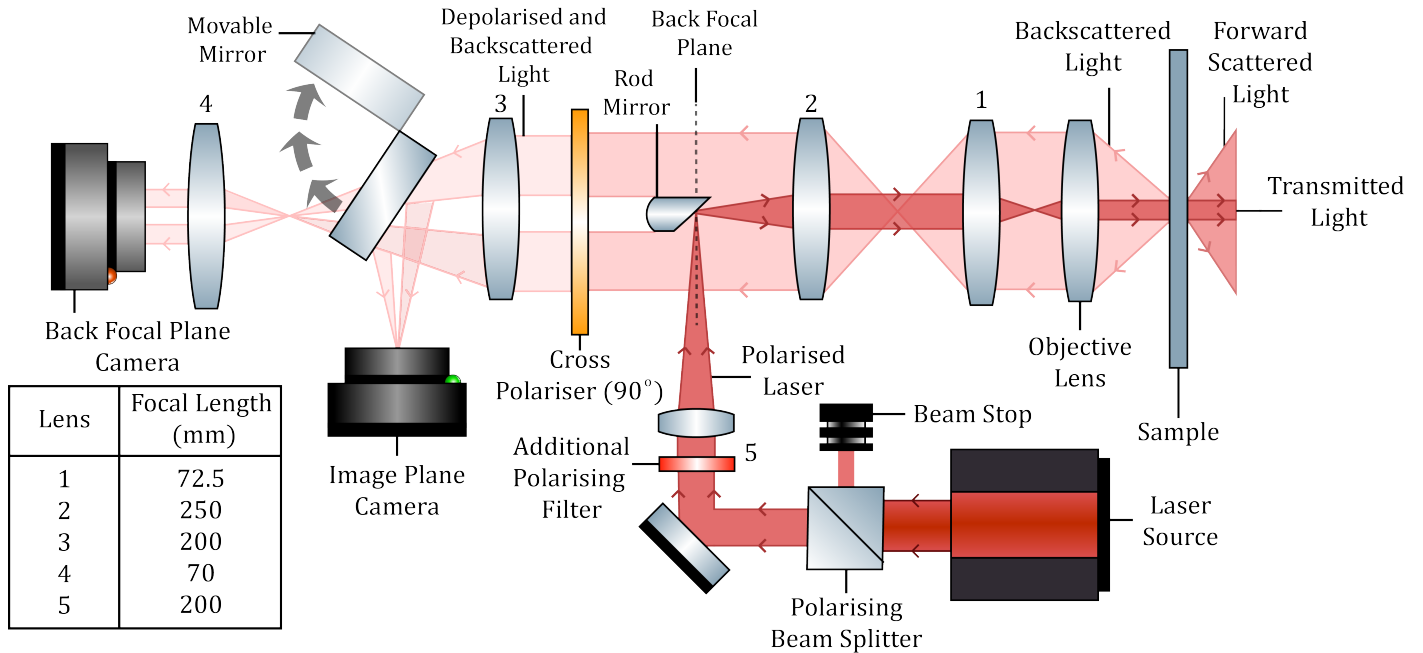
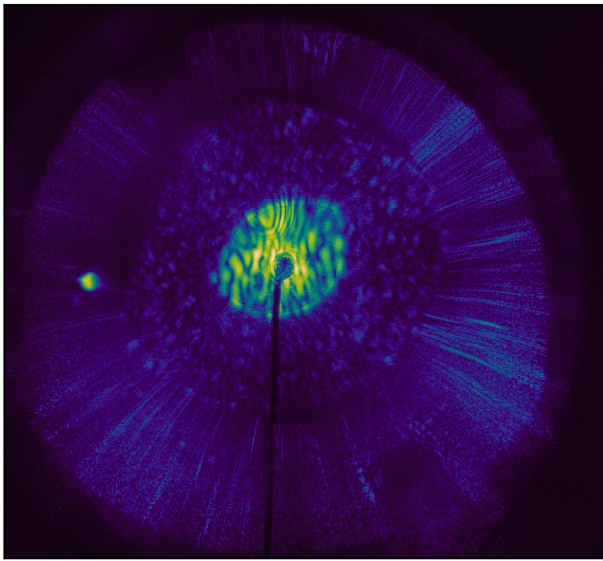


Figure 8: The BSDF setup with cross polarisers including lens focal distances.

Example On Axis BFP Image of an Isotonic Buffer Sample with NA 0.53 Lens



Example On Axis BFP Image of an Infected Thin Smear with NA 0.53 Lens

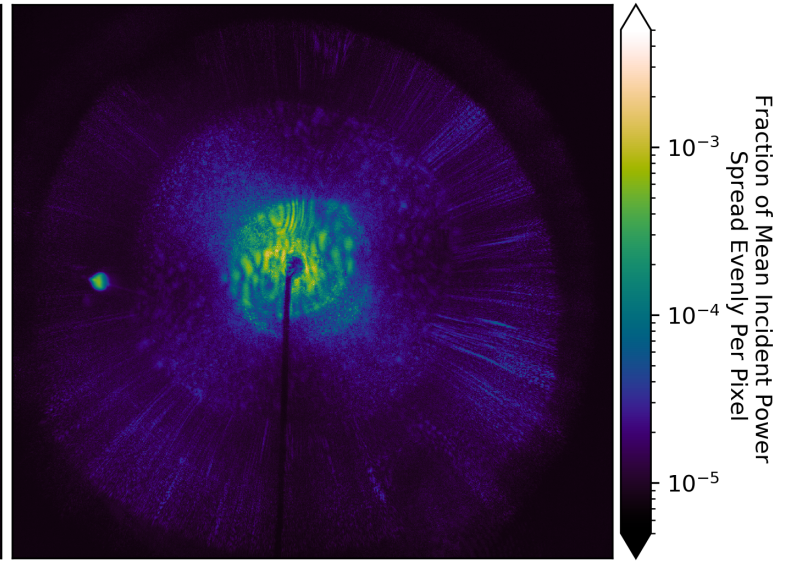


Figure 9: A comparison of a BFP image of isotonic buffer vs that of an infected thin smear. Note the cross pattern of increased intensity in the infected thin smear. This is a characteristic pattern of observing depolarised light and is called a Maltese cross.

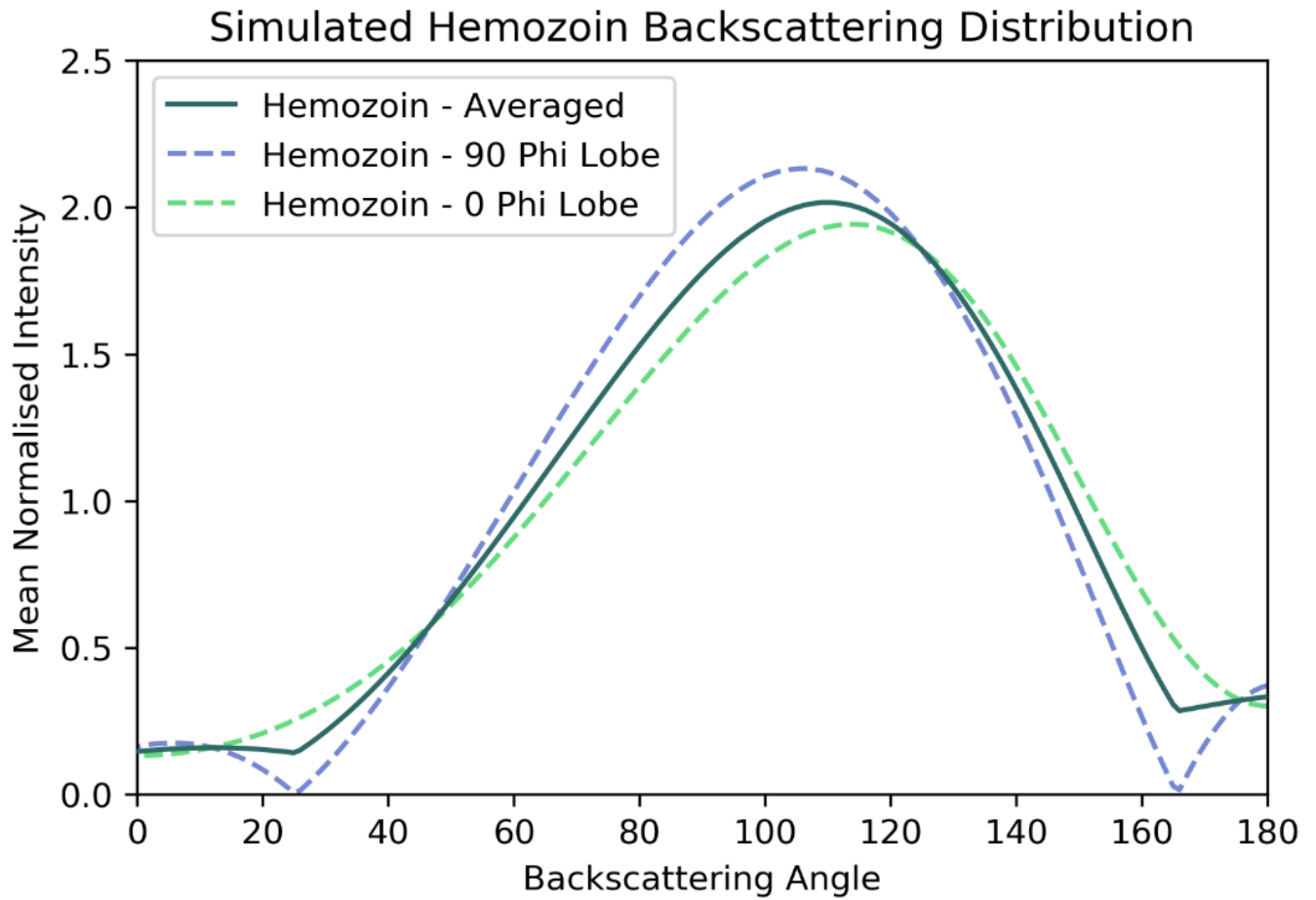


Figure 10: Two cross sections of a rectangular prism's (a model of hemozoin) depolarised backscattering distribution are modelled using DDA. The intensity is normalised such that the mean of each curve is equal to one.

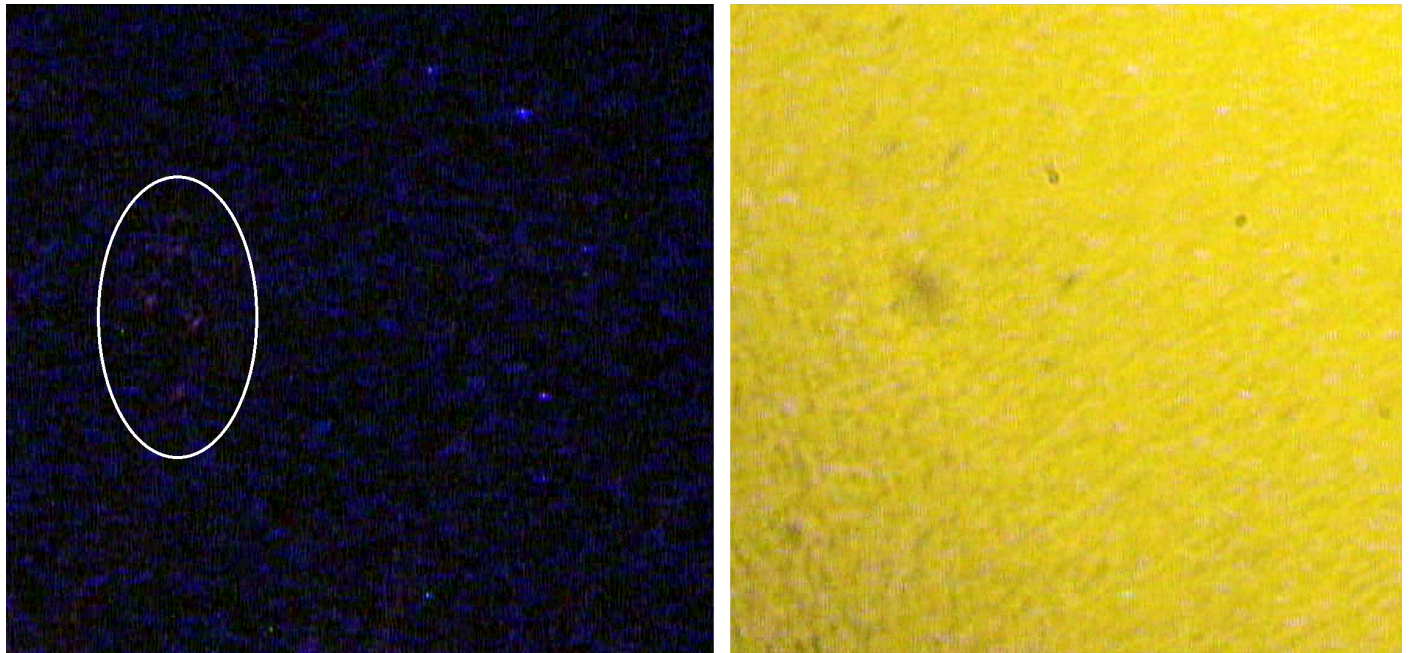


Figure 11: A still from a video of an infected thin smear sample taken in off-axis illumination with a NA 0.26 lens and BFP mask in which the image is switched from dark to bright field. Red dots show depolarised backscatter, the bright field image is taken using a yellow lamp as a light source. The small black dots in the bright field image are RBCs. The diffuse dark smudge is a smudge on the camera. In the dark field image the blue dots are noise that vary rapidly, when the camera is moved the diffuse smudges move with the field of view whilst the RBCs and regions of localised backscatter do not, indicating that the backscatter is originating from RBCs within the sample.